High-Density Stretchable Electrode Grids for Chronic Neural Recording

Klas Tybrandt,* Dion Khodagholy,* Bernd Dielacher, Flurin Stauffer, Aline F. Renz, György Buzsáki, and János Vörös

Electrical interfacing with neural tissue is key to advancing diagnosis and therapies for neurological disorders, as well as providing detailed information about neural signals. A challenge for creating long-term stable interfaces between electronics and neural tissue is the huge mechanical mismatch between the systems. So far, materials and fabrication processes have restricted the development of soft electrode grids able to combine high performance, long-term stability, and high electrode density, aspects all essential for neural interfacing. Here, this challenge is addressed by developing a soft, high-density, stretchable electrode grid based on an inert, high-performance composite material comprising gold-coated titanium dioxide nanowires embedded in a silicone matrix. The developed grid can resolve high spatiotemporal neural signals from the surface of the cortex in freely moving rats with stable neural recording quality and preserved electrode signal coherence during 3 months of implantation. Due to its flexible and stretchable nature, it is possible to minimize the size of the craniotomy required for placement, further reducing the level of invasiveness. The material and device technology presented herein have potential for a wide range of emerging biomedical applications.

Dr. K. Tybrandt, Dr. B. Dielacher, Dr. F. Stauffer, A. F. Renz, Prof. J. Vörös
Institute for Biomedical Engineering
ETH Zurich
8092 Zurich, Switzerland
E-mail: klas.tybrandt@liu.se

Dr. K. Tybrandt
Laboratory of Organic Electronics
Department of Science and Technology
Linköping University
601 74 Norrköping, Sweden

Dr. D. Khodagholy
Department of Electrical Engineering
Columbia University
New York, NY 10027, USA
E-mail: dion@ee.columbia.edu

Dr. D. Khodagholy, Prof. G. Buzsáki
NYU Neuroscience Institute
School of Medicine
New York University
New York, NY 10016, USA

Electrical stimulation has successfully been applied to treat neurological disorders like Parkinson's disease, epilepsy, hearing loss, and chronic pain. One reason for this success is that electrical stimulation can compensate for scar tissue encapsulation of electrodes by increasing the stimulation current and thereby continuing to reach the stimulation threshold.[1] However, current and emerging therapies would benefit from the use of closed feedback systems, in which recorded signals are used to control the stimulation for optimal effect.[2,3] This approach requires the establishment of a well-integrated, long-term stable, electronic–neural interface to pick up weak neural signals. One major factor which restricts the long-term stability of neural interfaces is the huge mechanical mismatch between electronics and neural tissue.[4] Even plastic substrates exhibit elastic moduli in the GPa range, while neural tissue is viscoelastic with elastic moduli in the kPa range.[5] As neural tissue constantly endures bodily motions and deformations, stiff implants will cause mechanical wear at the interface, leading to tissue responses with deteriorating performance of the implant.[4,6–8] To avoid this effect, neural implants need to be engineered out of materials that match the mechanical properties of the interfaced tissue as closely as possible.[9–11] Flexible electrode grids[12,13] and penetrating probes[14,15] have been developed to improve the electrode–tissue interface. In recent years, further steps in this direction have been taken by the development of soft and stretchable electrically conductive composites, typically comprising a conductive filler embedded in an elastomer matrix.[16–21] Biomedical implants have a strict set of material requirements, including long-term stability, nontoxicity, and biocompatibility. This disqualifies most reported composites, as silver is unstable and toxic,[1,10] while carbon nanotube based composites require detergents/ionic liquids that may leak out into the tissue.[18] Microcracked gold is to date the premier example of an implantable stretchable conductor,[22,23] and it has been used to fabricate soft and stretchable electrode arrays for stimulation and recording.[11] Although very useful, microcracked gold has high sheet resistance and reported fabrication protocols have not allowed for the far-reaching miniaturization necessary for high-resolution neural recording. To tackle these limitations, here we report on the development of a novel inert high-performance

**ADVANCED
SCIENCE NEWS**

www.advancedsciencenews.com

**ADVANCED
MATERIALS**

www.advmat.de

stretchable conductor and the corresponding device technology for high-density, stretchable electrode grids (SEGs) for neural recording. The composite is based on gold-coated titanium dioxide nanowires (Au-TiO$_2$NWs), and has good conductivity, electromechanical properties, and long-term stability. Based on this material, we present a miniaturized soft SEG device technology, which exhibits the highest electrode density of any SEG to date. This feature allows us to chronically implant the device onto the somatosensory cortex in freely moving rats and record high spatiotemporal neural signals during 3 months of implantation. The benefits of the soft and stretchable device technology are also manifested as conformal contact to the tissue and self-expansion after insertion through a smaller cranial window than the probe geometry.

To avoid any potentially toxic seed particles or capping agents, we utilized titanium dioxide nanowires (TiO$_2$NWs) as the starting material (Figure S1, Supporting Information). The TiO$_2$NWs were dispersed in a mixture of the biocompatible capping agent poly(vinylpyrrolidone) (PVP) and the mild reducing agent hydroxylamine (HDA), followed by addition of chloroauric acid (HAuCl$_4$) solution to the mixture under stirring via a syringe pump (**Figure 1**a). The optimized procedure resulted in a conformal coating of gold on the TiO$_2$NWs (Table S1, Supporting Information). To stabilize the nanowire dispersion, hydrochloric acid was subsequently added, which also resulted in a color change from grey–brown to orange–red over a few days (Figure 1b). The Au-TiO$_2$NWs sedimented within an hour, but could be redispersed even after half a year without any noticeable aggregation. The growth process of the gold was studied by extracting samples at various stages of the coating process.

When 1/10 of the gold salt had been added, the TiO$_2$NWs were partially covered by a thin layer of gold (Figure 1c). Once all gold salt had been reduced, the TiO$_2$NWs were fully covered by a rough layer of gold (Figure 1d,e). A week after adding the hydrochloric acid, the roughness of the gold coating had decreased significantly (Figure 1e). For electrical characterization, samples of 0.5 mm width and 20 mm length were prepared by masked vacuum filtration.[24] First, the nanowire dispersion was filtered through, followed by a rinsing step of phosphate-buffered saline (PBS) filtration and drying on a hotplate. Samples prepared from fresh dispersions showed decreasing sheet resistance over time (Figure 1f). A similar trend emerged for samples prepared from stored dispersions (Figure 1f). Stretchable samples were fabricated by transferring the Au-TiO$_2$NW patterns from the filter membranes to semi-cured poly(dimethylsiloxane) (PDMS) substrates, followed by spin coating of a top PDMS layer to encapsulate the Au-TiO$_2$NW tracks. The initial sheet resistance of the ≈3 µm thick tracks was 0.63 ± 0.03 Ω □$^{-1}$, which translates into a conductivity of ≈16000 S cm^{-1}. When stretched, the sheet resistance increased to ≈3 Ω □$^{-1}$ for 50% strain and ≈7 Ω □$^{-1}$ for 100% strain. Some samples started to lose electrical contact above 100% strain, and the samples broke mechanically between 150% and 200% strain. The composite showed excellent strain cycling stability when cycled to 20%, 50%, and 100% strain 1000 times (Figure 1h). The addition of Au-TiO$_2$NWs only caused a minor (12%) stiffening of the samples at 50% strain (Figure S2, Supporting Information).

To fabricate high-density SEGs, we employed a recently developed method based on photolithographic masking of filter
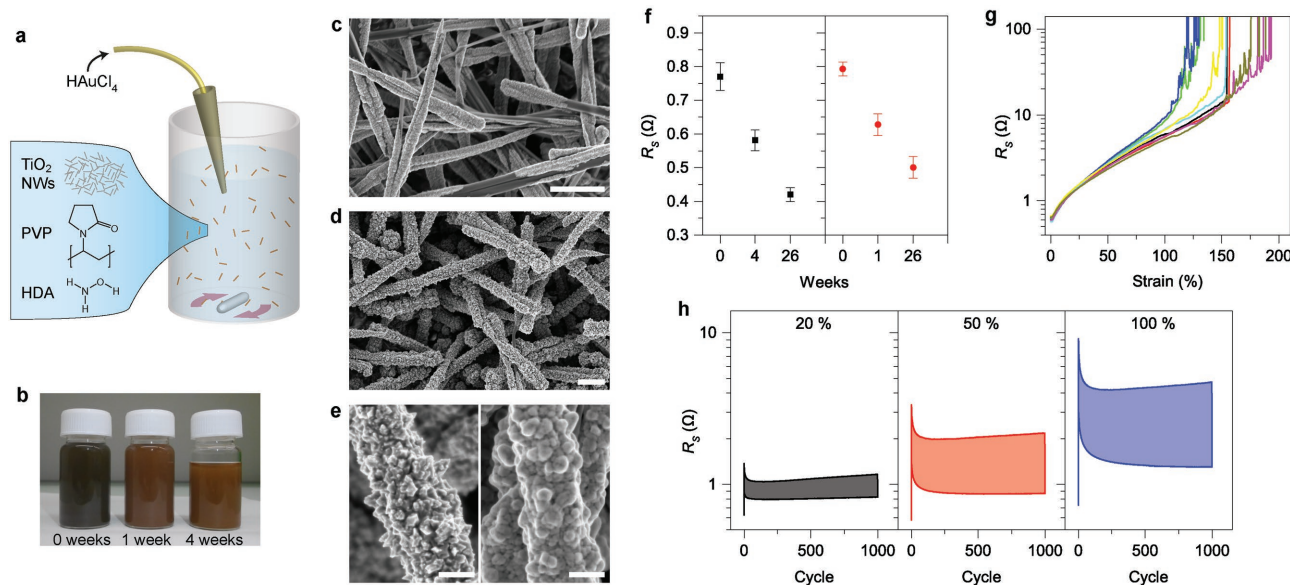
Figure 1. Stretchable Au-TiO$_2$NW-PDMS composite. a) The TiO$_2$NWs are coated with gold by reducing HAuCl$_4$ salt with HDA in the presence of a capping agent (PVP). b) The addition of HCl stabilizes the dispersion and promotes a color change from brown–grey to orange–red. c–e) SEM images of the Au-TiO$_2$NWs at different stages during the coating process. c) A partial gold coating is produced when 1/10 of the gold salt solution has been added. d) At the end of the reaction, a continuous gold coating has been produced. e) The initial gold coating is rough (left), but smoothens out after one week (right). f) The sheet resistance R_S of films made from freshly produced Au-TiO$_2$NWs improves over time (■). The conductivity of the NWs stored in the dispersion improves over time as well (●). g) Stretchable conductors are produced by embedding the NWs in PDMS. The sheet resistance remains below 10 Ω □$^{-1}$ up to 100% strain. h) The conductors show excellent stability for 1000 strain cycles at 20%, 50%, and 100% strain. Scale bars: c,d) 500 nm, e) 200 nm.
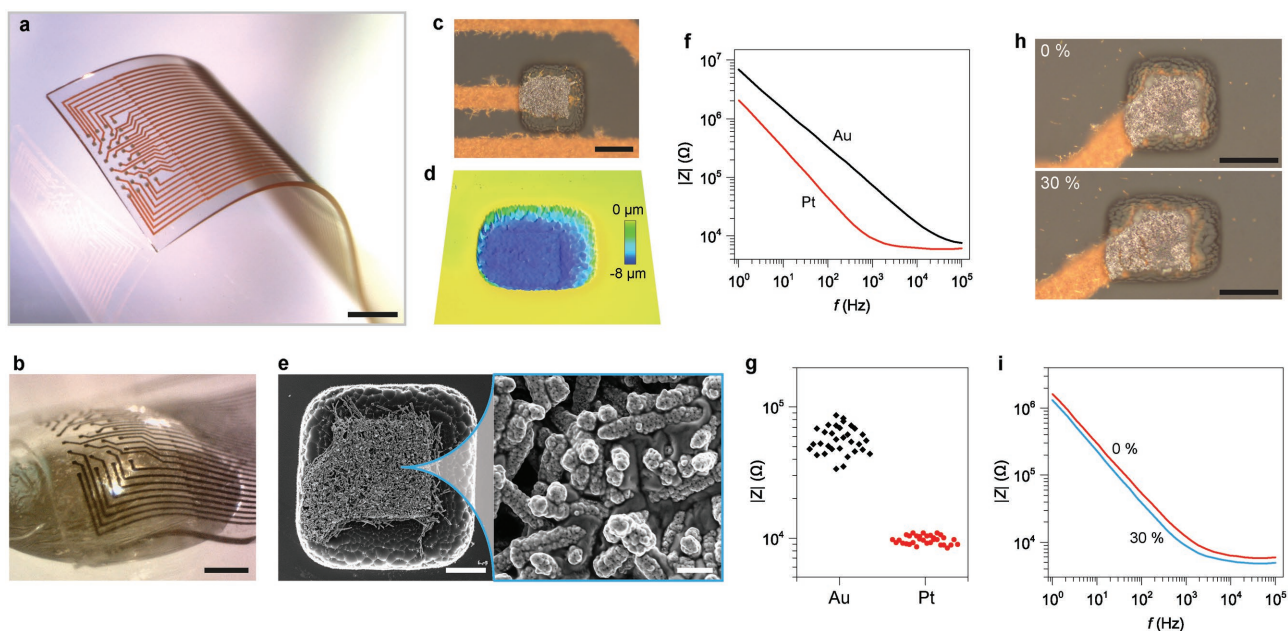
Figure 2. Soft and stretchable electrode grids. a) The electrode grid is made of Au-TiO$_2$NW conductors embedded in PDMS and comprises 32 electrodes with 200 µm pitch. b) The stretchability allows the SEG to establish conformal contact around curved surfaces. c) An opening in the PDMS layer is etched to form the 50 µm large electrodes. A thin layer of platinum is electroplated onto the exposed Au-TiO$_2$NWs to improve electrode performance. d) Optical surface profilometry reveals that the electrode openings are ≈7 µm deep. e) The SEM image of the electrode shows how the Pt-coated Au-TiO$_2$NWs are partially embedded in the PDMS. f) The impedance of the electrode before (—) and after (—) electroplating of platinum. g) Measured impedance at 1 kHz of the electrodes of an SEG before (♦) and after (●) Pt coating. h) Microscopy images of the electrode at 0% and 30% strain. i) The impedance of an electrode at 0% (—) and 30% (—) strain. Scale bars: a) 1 mm, b) 500 µm, c) 50 µm, e) 20 µm and 1 µm, h) 50 µm.

membranes.[25] The method can produce arbitrary nanowire patterns down to 20 µm sized features and yields high performance, narrow, stretchable conductor lines. The Au-TiO$_2$NW dispersion was filtered through the masked membrane, cleaned by filtering of PBS buffer, dried, and then transferred to a semi-cured PDMS substrate (≈75 µm thick). The membrane was wetted from the backside and peeled off, leaving the transferred pattern on the PDMS substrate. Next, a thin top layer of PDMS (≈6 µm) was spin coated onto the substrate and cured. Electrodes and contacts were created by patterning of a dry film resist followed by dry etching until the Au-TiO$_2$NWs were exposed. Finally, the SEG was clamped on a custom-made connector and a thin layer of platinum was electroplated onto the exposed Au-TiO$_2$NWs to form the electrodes (Figure S3, Supporting Information). The resulting soft SEG is shown in **Figure 2**a and was ≈80 µm thick and 3.2 mm wide at the tip (see Figure S4 in the Supporting Information for full fabrication scheme). The SEG had 8 × 4 electrodes with 200 µm electrode spacing, enabled by the 30 µm wide conductor lines (Figure S5, Supporting Information). The softness and stretchability allowed the SEG to conform to curvilinear shapes (Figure 2b). The electrodes were ≈50 × 50 µm in size (Figure 2c), and the electrode openings were ≈7 µm deep (Figure 2d). SEM images revealed the nanostructure of the electrodes, in which the platinum coated nanowires were partially embedded in the PDMS underneath them (Figure 2e, Figure S6, Supporting Information). The platinum coating decreased the impedance of the electrodes by a factor of 5 (Figure 2f,g), resulting in an areal capacitance of ≈2.7 mC cm^{-2}. The plating process also improved the electrode stability during electrical stimulation, with no

degradation in performance after 10^6 bipolar pulses (1 V, 200 µs) of the physiologically relevant current range of 100 µA (Figure S7, Supporting Information). When the electrodes were stretched to 30% strain (Figure 2h), the impedance decreased slightly in accordance with the increase in electrode area (Figure 2i). A batch of 16 SEGs was fabricated for this study, of which 7 devices were fully functional. The defective SEGs had a few breaks on the narrow conductor lines and were therefore discarded.

In vivo evaluation and characterization of the SEGs were carried out in rats by implanting probes on the somatosensory cortex (**Figure 3**a) to record somatosensory evoked potentials (SSEPs).[26] The recordings were performed both acutely in the intraoperative setting, as well as chronically in freely moving rats (Figure 3c), to further characterize the spatiotemporal resolution of neural signals captured by the soft and stretchable probes. Owing to the softness and stretchability of the SEG, it could be folded on itself and inserted through an ≈30% narrower craniotomy window than its original size. Once inserted, the grid self-expanded onto the pial cortical surface (Figure 3b). For chronic in vivo recording, the grid was covered with a piece of bioabsorbable gelatin compressed sponge (Gelfoam) and the craniotomy was sealed with silicone elastomer. Physiological recordings were performed while rats engaged in normal behavior in their home cage, and intraoperative recordings were carried out under isoflurane anesthesia. Neural signals were amplified, multiplexed and digitized using a head-stage mounted directly on the grid to minimize environmental noise contamination.

SSEPs were performed by insertion of two 36 AWG gold plated wires into the hind limb of the rat contralateral to the
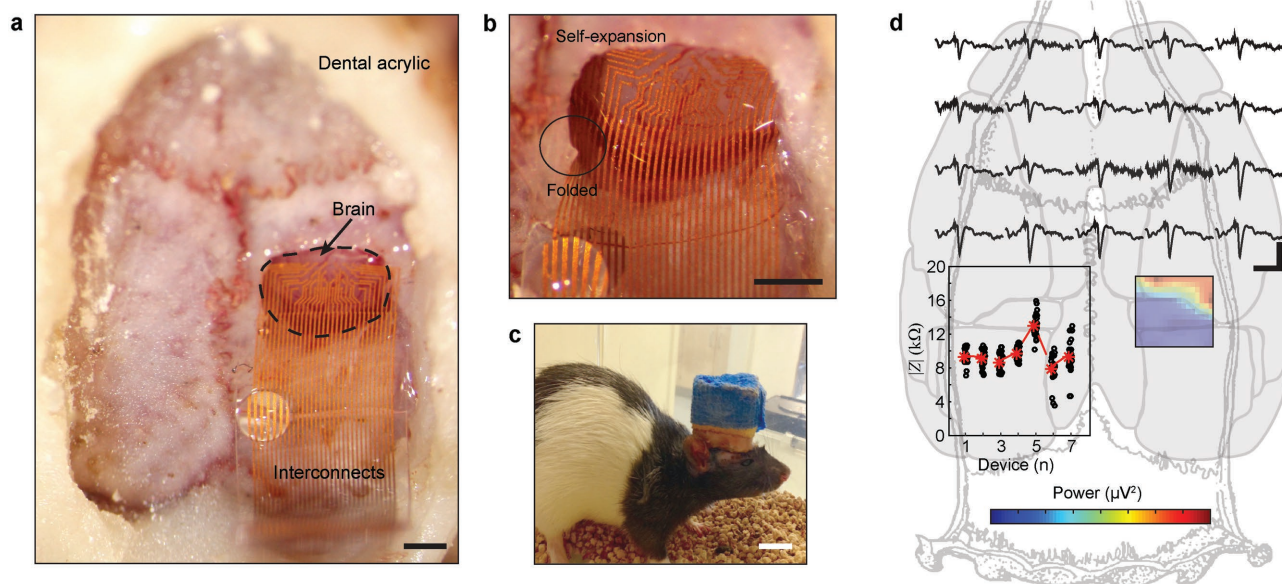
Figure 3. Implantation and in vivo neural recording of soft SEGs. a) Intraoperative microphotograph of soft SEG showing the probe in a craniotomy lying on the surface of the brain. Note the hydrophobic nature of the device demonstrated by a drop of water on the ribbon area. b) Zoomed-in microscopy image showing the ability of the probe to be inserted in smaller craniotomy than the probe geometry. c) Freely moving rat with chronically implanted SEG. d) Intraoperative recording of SSEPs using the soft SEG. Top: raw LFP time traces showing SSEPs generated by hind limb electrical stimulation. Right: heat map demonstrating the anatomical localization of SSEPs to the somatosensory cortex. Left: electric impedance of the SEGs at 1 kHz, showing a uniform impedance range across devices. Scale bars: a,b) 1 mm, c) 10 mm, d) 100 ms, 500 µV.

craniotomy location under isoflurane anesthesia. Current pulses with 1 ms duration were titrated until movement of the digits was visually observable. Pulses were repeated every 3 s for 10–15 min. Figure 3d illustrates the unfiltered SSEP time traces recorded by the SEG with clear spatial patterning of the evoked potential. Furthermore, such a spatial gradient is consistent with the anatomical placement of the probe, illustrated by the heat map on the dorsal view of the rat skull. Importantly, throughout the recording, the majority of the electrodes (>85%) were functional and exhibited similar electrical impedance, highlighting the reliability of the fabrication process of the SEGs.

To further explore the capacity of the soft SEGs, the devices and the data generated by them should be validated for systems neuroscience contexts and experiments. Furthermore, for neural recordings to be maximally useful, they should be stable over time. The intraoperative recordings demonstrated that soft SEGs can generate high signal to noise ratio neural data. Therefore, we moved forward to record high spatiotemporal resolution signals in chronic preparations over an extended period of time. **Figure 4**a,b shows a sleep epoch acquired by the SEG that consists of sleep spindle (σ) and gamma (γ) oscillations during nonrapid eye movement (NREM) sleep epochs, and theta (θ) and gamma oscillations during rapid eye movement (REM) sleep epochs. The ability to capture these oscillations in chronic experiments highlights the stability of the recording, and health of the surrounding neural tissue. At a finer timescale, these recordings revealed several high-frequency oscillations with defined spatial extent localized on the SEG (Figure 4c). Due to the high-density and large spatial coverage of the electrodes of the SEG, we could investigate the spatial extent of these oscillations by determining the coherence over distance

for various frequency bands (1 to 90 Hz) in the chronically implanted SEG (Figure 4d). As predicted by theoretical models of the spatial scale of the local field potential (LFP),[27,28] coherence was high at low frequencies and decreased for higher frequencies, highlighting the physiological nature of these oscillations. Moreover, these analyses suggested that LFP patterns can be differentiated at sub-millimeter distances and that high spatiotemporal resolution sampling of neural activity can provide information about physiological cortical processes. The recording quality was stable over time, as the average power of the recorded signals was similar after 1, 2, and 3 months of implantation (Figure 4e). After 3 months, 28 electrodes showed excellent signal quality, 3 had weaker signals, and only one electrode was dead (Figure 4f, Figure S8 in the Supporting Information). As the failing electrodes were not adjacent to each other, but connected next to each other on one side of the connector (Figure S4, Supporting Information), it is likely that the failure is related to the grid-connector contact rather than the stretchable conductor or the electrode–tissue interface.

The coating of the TiO$_2$NWs starts by the formation of a thin, partially covering gold layer. As the pH of the dispersion ranges from 6 to 7 during the synthesis, the titanium dioxide is neutral[29] while the gold (nanoparticles) are negatively charged.[30] As PVP further reduces any surface charge, the adsorption of the initial gold layer is thus probably not driven by electrostatic forces, but rather by van der Waal's attraction. This hypothesis suggests that other template materials, like carbon nanotubes or fibers, could be used in a similar fashion, although little gain in performance would be expected due to the superior conductivity of gold. The coating process is effective, as no free gold (nano)particles can be seen in the SEM images or in the filtrate. This is probably due to the chosen reducing agent's

**ADVANCED
SCIENCE NEWS**

www.advancedsciencenews.com

**ADVANCED
MATERIALS**

www.advmat.de
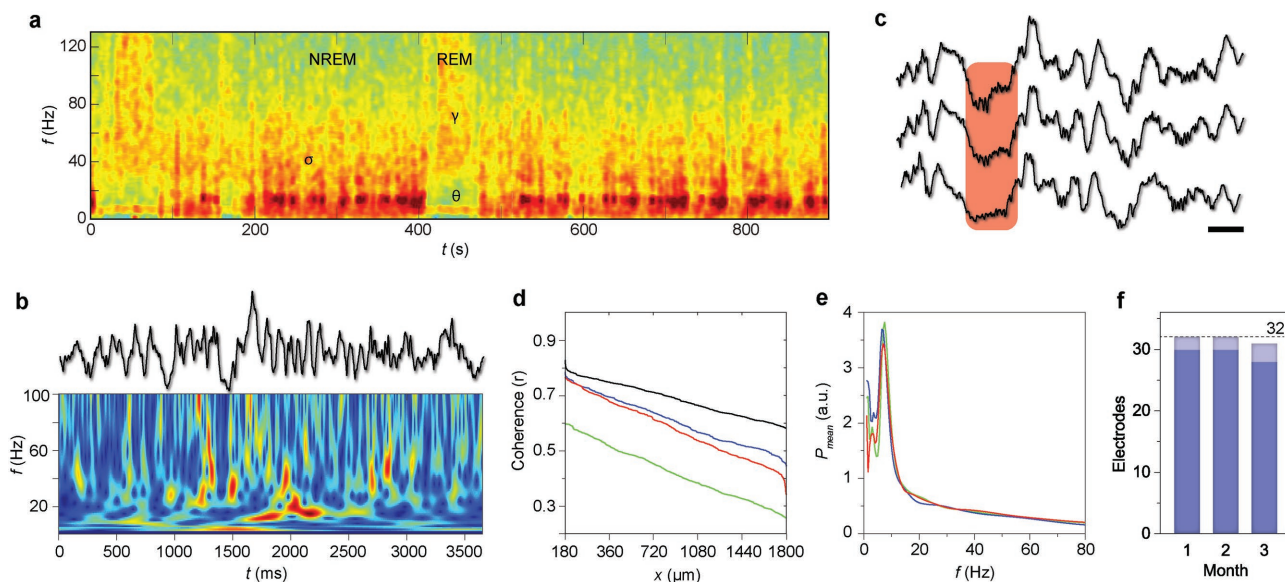
Figure 4. In vivo chronic recording and spatial distribution of local field potential. a) Time–frequency spectrogram of LFP recorded by the soft SEG during sleep in somatosensory cortex. The spectrogram during an NREM epoch contains slow oscillations (2–4 Hz) and sleep spindles (9–16 Hz); during a REM epoch theta (4–8 Hz) and gamma (30–80 Hz) oscillations were seen. Colors represent normalized power, with warmer colors indicating higher power. b) Raw LFP trace (top) and corresponding spectrogram (bottom) from 3 month chronically implanted SEG during an NREM epoch. c) Raw LFP trace highlighting a spatially patterned gamma oscillation during an NREM epoch. d) Average coherence between recording electrodes at each frequency band in an NREM session (— 2–4 Hz), (— 4–8 Hz), (— 9–16 Hz), (— 30–80 Hz). e) Mean power of recorded signal after 1 (—), 2 (—), and 3 (—) months of implantation. f) Number of functional recording electrodes after 1, 2, and 3 months of implantation, with high-quality recording electrodes in blue and low-quality recording electrodes in light blue. Scale bar: c) 100 ms.

surface-catalyzed reduction of Au^{3+}, which prevents continuous seeding of new gold nanoparticles.[31] The addition of HCl to the dispersion induces a gradual color change, which is caused by smoothening of the initially rough gold surface. The smoothening improves the electrical conductivity, giving the Au-TiO_2NW-PDMS composite a conductivity of ≈16000 S cm^{-1}, which compares well with previously reported stretchable composites.[16,17,20,32] Even better, the electromechanical characteristics remain stable after one thousand strain cycles of 100% strain, which is important for a material considered for long-term use. A possible explanation for this advantageous behavior is the small size of the cracks in the composite under strain (Figure S9, Supporting Information) in comparison to silver nanowire-based composites.[24] This observation might in turn be related to the relatively low degree of stiffening caused by the Au-TiO_2NWs.

The fact that Au-TiO_2NWs are long-term stable and can be dispersed in water without ultrasonication makes the material convenient to use. Further, the developed filtration method exhibits certain advantages for biomedical applications: (i) the material consumption is low which allows for the use of expensive noble metals; (ii) the nanowires can easily be cleaned in the process, thereby removing potentially harmful chemicals; (iii) the method yields high-quality micro-patterns that enable high electrode density; (iv) PDMS or other medical grade silicones can be used in the process; (v) the patterning process does not expose the sensitive PDMS substrate to any aggressive organic solvents or potentially harmful substances. The impedance of the microelectrodes is around 10 kΩ at 1 kHz in PBS, which is low enough for high-quality recordings. When

fitting an equivalent circuit to the impedance data (Figure S10, Supporting Information), a constant phase element is needed. This indicates that the electrodes are porous, which is in line with the high areal capacitance (2.7 mC cm^{-2}) and the SEM images. Our SEG outperforms previously reported devices in terms of electromechanical properties, electrode density, and electrode performance (**Table 1**), all key features for high-quality neural recording. Also, our SEG has demonstrated stable neural recordings for the longest period of any implanted SEG. Although nanomaterials are great for electrode performance, one need to consider the risk of nanotoxicity, often mediated through the creation of reactive oxygen species (ROS).[33] TiO_2 nanoparticles have been found to cause relatively low levels of ROS induced stress in cells.[34,35] However, this should not be an issue in this work as the electrodes and Au-TiO_2NWs can be fabricated without any visible exposure of TiO_2 (Figure S6, Supporting Information). Overall, these features make the developed technology a premier candidate for a wide range of biomedical applications.

The soft and stretchable nature of the SEG allowed us to perform craniotomies that were smaller than the probe's geometry, reducing the risk of surgical complications and cerebral swelling. Moreover, the hydrophobic surface of the probe provided an efficient contact with the brain and minimized the cerebrospinal fluid shunting effect across electrodes. This was highlighted by localization of the somatosensory potentials during acute recording and high-frequency oscillations during chronic recordings. The fabrication process produced high-density grids with large spatial coverage that allowed determination of the spatial extent of brain oscillations for various frequency bands

**ADVANCED
SCIENCE NEWS**

www.advancedsciencenews.com

**ADVANCED
MATERIALS**

www.advmat.de

Table 1. Comparison between the SEG in this work and previously reported SEGs.

Conductor	R_S [Ω]	Max strain [%]	Electrode material	Electrode count	Electrode density[c] [mm^{-2}]	Electrode size [10^3 μm^2]	$|Z|$[d] at 1 kHz [kΩ]	$|Z| \cdot A$[e] at 1 kHz [kΩ cm^2]	Implantation period [weeks]	Ref.
Au-TiO^2-NWs	0.6	100	Pt plated NWs	32	38	3	10	0.3	13	This work
PPy/PCTC	6	23	PPy/PCTC	4	0.2	800	10	80	Acute	[36]
PPy/PTSA	8	9[b]	PPy/PTSA	4	0.9	200	30	60	Acute	[37]
Au film 35 nm	9[a]	>45	Pt-PDMS	9	3	70	3	2	6	[11]
Au film 50–150 nm	-	≈10	Au	11	3	3	200	6	in vitro	[38]
Au film 38 nm	–	≈10	Pt	28	11	10	100	10	in vitro	[39]

[a] R_S not given, adopted from ref. [22]; [b] In prestrained device 110%; [c] Area calculated from rectangle enclosing the electrodes; [d] $|Z|$ is impedance; [e] Areal impedance.

(1–90 Hz) at sub-millimeter resolution. In clinical practice, grid arrays can provide a 2D localization of epileptic foci. However, obtaining such information can be limited by the size of the cranial window required to insert such an array. The ability of the SEGs to be inserted through smaller cranial windows would potentially enable acquisition of such spatial data while reducing the size of the cranial window. Altogether, we believe that the presented technology constitutes an attractive platform for the continued development of mechanically compliant neuronal probes for long-term recording. Specifically, the adaptation of the technology to penetrating probes should be especially rewarding due to the softness and deformability of the probes.

Experimental Section

Au-TiO$_2$NWs: TiO$_2$ nanowires (ACSMaterial, TiO$_2$NW-A, length ≈10 μm, 0.15 mg), hydroxylamine (Sigma-Aldrich, 50%, 61 μL), and poly(vinylpyrrolidone) (Sigma-Aldrich, MW 50k, 0.33 g) were mixed with deionized (DI) water to a final volume of 9.5 mL. Gold(III) chloride solution (Sigma-Aldrich, Au 17 wt%, 61 μL) was diluted in DI water to a final volume of 10 mL. The gold solution was added with a syringe pump into the TiO$_2$NW solution under stirring (1 mL at 1.4 mL min^{-1}, then 9 mL at 0.7 mL min^{-1}). Hydrochloric acid (Sigma-Aldrich, 37%, 0.5 mL) was added 5 min after completion. The dispersion was put through a 20 μm stainless steel sieve to remove eventual large aggregates. The dispersion was stored for at least 1 d before use. SEM images were taken with a Zeiss Leo 1530.

Electromechanical Characterization: Au-TiO$_2$NW tracks (20 mm length, 0.5 mm width) with contact pads were patterned by wax assisted vacuum filtration[24] (4 mL Au-TiO$_2$NW solution, 200 mm^2 open filter area) and transferred to a semi-cured PDMS sample (Sylgard 184, Dow Corning, 1:10, 1 krpm spin speed, 30 s, 6 min 70 °C curing). A diluted PDMS solution (PDMS:heptane 1:20) was spin coated (6 krpm 60 s) to reinforce the contact pads and cured (80 °C, 20 min). A 25 μm poly(ethylene naphthalate) foil was used to mask the contact pads and a layer of PDMS was spin-coated on top (2 krpm 30 s). The foil was removed and the samples were cured (80 °C, 16 h). The samples were clamped in a tensile testing machine (DO-FB0.5TS, Zwick/Roell) with copper tape as contacts. A digital multimeter (Agilent 34401A) was used to measure the resistance at 4 Hz. The strain rate was 0.5 mm s^{-1} for the maximum strain tests and 2 mm s^{-1} for the cycling tests.

SEG Fabrication and Characterization: Hydrophilic PVDF membranes (0.22 μm pore size, Millipore) were patterned with ma-N 490 photoresist (micro resist technology GmbH) according to previously published protocol.[25] Au-TiO$_2$NW dispersion (1.8 mL, 92 mm^2 open filter area) followed by PBS buffer (10 mL) was vacuum filtered through the patterned membrane. PDMS was spin-coated (Sylgard 184, 1 krpm spin speed, 30 s) onto a silanized 2 inch glass wafer and semi-cured

(70 °C, 6 min). The dried membrane was put in contact with the PDMS under pressure (80 °C, 10 min) and peeled off after being soaked in DI water. A diluted PDMS solution (PDMS:heptane 1:20) was spin coated (6 krpm 60 s) and cured (80 °C, 20 min), followed by another spin-coated PDMS layer (6 krpm, 120 s) and curing (80 °C, 16 h). After 10 min UV ozone treatment, a poly(vinyl alcohol) (PVA) layer was spin-coated on top (10%, 3 krpm, 60 s). A dry film resist layer was laminated on top (LP Dry Film Photopolymer), exposed, and developed. The substrate was dry etched (RIE, 250 W, 100 mTorr, O$_2$/CF$_4$, 400 s) and the PVA and dry resist stripped in boiling DI water. The SEG was cut out with a scalpel and clamped on a custom-made printed circuit board connector. Finally, a thin layer of platinum was electroplated onto the electrodes (Sigma-Aldrich, chloroplatinic acid solution 0.8 wt% in DI water, pulsed −1.5 V, 20 Hz, 10% duty cycle).

Animal Surgical Procedure: All animal experiments were approved by the Institutional Animal Care and Use Committee at New York University Langone Medical Center. Three male rats (200–350 g, 8–15 weeks of age) were used for SEG acute and chronic implantations. Rats were kept on a regular 12–12 h light–dark cycle and housed in pairs before implantation, but separated afterward. No prior experimentation had been performed on these rats. The animals were initially anaesthetized with 2% isoflurane and maintained under anesthesia with 0.75–1% isoflurane during the surgery. A 2 × 3 mm^2 craniotomy over somatosensory cortex (AP -3.0 ML 3.5) was performed. This was followed by dura-mater removal, resulting in an effective 2 × 2.5 mm^2 exposed brain surface. The SEG was folded and inserted into the craniotomy and self-expanded onto the pial surface of the brain. After all surgical procedures, the craniotomies were covered with gel-foam and sealed using a silicone elastomer. Once the rats had recovered for 5 d postsurgical procedure, somatosensory evoked potentials were performed by insertion of two 36 AWG gold plated wires into the hind limb of the rat contralateral to the cranial window under isoflurane anesthesia. Current pulses with 1 ms duration were titrated until movement of the digits was visually observable. Pulses were repeated every 3 s for 10–15 min.

Supporting Information

Supporting Information is available from the Wiley Online Library or from the author.

Acknowledgements

Conflict of Interest

The authors declare no conflict of interest.

Keywords

[1] D. R. Merrill, M. Bikson, J. G. R. Jefferys, *J. Neurosci. Methods* **2005**, *141*, 171.

[2] E. Krook-Magnuson, J. N. Gelinas, I. Soltesz, G. Buzsaki, *JAMA Neurol.* **2015**, *72*, 823.

[3] R. A. Normann, *Nat. Clin. Pract. Neurol.* **2007**, *3*, 444.

[4] S. P. Lacour, G. Courtine, J. Guck, *Nat. Rev. Mater.* **2016**, 1.

[5] S. Cheng, E. C. Clarke, L. E. Bilston, *Med. Eng. Phys.* **2008**, *30*, 1318.

[6] S. R. Goldstein, M. Salcman, *IEEE Trans. Biomed. Eng.* **1973**, *20*, 260.

[7] L. Hyunjung, V. B. Ravi, S. Wei, E. L. Marc, *J. Neural. Eng.* **2005**, *2*, 81.

[8] C. B. James, A. Juan, P. D. John, *J. Neural. Eng.* **2016**, *13*, 026003.

[9] S. Il Park, D. S. Brenner, G. Shin, C. D. Morgan, B. A. Copits, H. U. Chung, M. Y. Pullen, K. N. Noh, S. Davidson, S. J. Oh, J. Yoon, K. I. Jang, V. K. Samineni, M. Norman, J. G. Grajales-Reyes, S. K. Vogt, S. S. Sundaram, K. M. Wilson, J. S. Ha, R. X. Xu, T. S. Pan, T. I. Kim, Y. G. Huang, M. C. Montana, J. P. Golden, M. R. Bruchas, R. W. Gereau, J. A. Rogers, *Nat. Biotechnol.* **2015**, *33*, 1280.

[10] J. Park, S. Choi, A. H. Janardhan, S.-Y. Lee, S. Raut, J. Soares, K. Shin, S. Yang, C. Lee, K.-W. Kang, H. R. Cho, S. J. Kim, P. Seo, W. Hyun, S. Jung, H.-J. Lee, N. Lee, S. H. Choi, M. Sacks, N. Lu, M. E. Josephson, T. Hyeon, D.-H. Kim, H. J. Hwang, *Sci. Transl. Med.* **2016**, *8*, 344ra86.

[11] I. R. Minev, P. Musienko, A. Hirsch, Q. Barraud, N. Wenger, E. M. Moraud, J. Gandar, M. Capogrosso, T. Milekovic, L. Asboth, R. F. Torres, N. Vachicouras, Q. Liu, N. Pavlova, S. Duis, A. Larmagnac, J. Vörös, S. Micera, Z. Suo, G. Courtine, S. P. Lacour, *Science* **2015**, *347*, 159.

[12] D. W. Park, A. A. Schendel, S. Mikael, S. K. Brodnick, T. J. Richner, J. P. Ness, M. R. Hayat, F. Atry, S. T. Frye, R. Pashaie, S. Thongpang, Z. Q. Ma, J. C. Williams, *Nat. Commun.* **2014**, *5*, 5258.

[13] D. Khodagholy, T. Doublet, P. Quilichini, M. Gurfinkel, P. Leleux, A. Ghestem, E. Ismailova, T. Herve, S. Sanaur, C. Bernard, G. G. Malliaras, *Nat. Commun.* **2013**, *4*, 1575.

[14] T. D. Y. Kozai, N. B. Langhals, P. R. Patel, X. P. Deng, H. N. Zhang, K. L. Smith, J. Lahann, N. A. Kotov, D. R. Kipke, *Nat. Mater.* **2012**, *11*, 1065.

[15] H. N. Zhang, P. R. Patel, Z. X. Xie, S. D. Swanson, X. D. Wang, N. A. Kotov, *ACS Nano* **2013**, *7*, 7619.

[16] F. Xu, Y. Zhu, *Adv. Mater.* **2012**, *24*, 5117.

[17] T. Sekitani, H. Nakajima, H. Maeda, T. Fukushima, T. Aida, K. Hata, T. Someya, *Nat. Mater.* **2009**, *8*, 494.

[18] T. Sekitani, Y. Noguchi, K. Hata, T. Fukushima, T. Aida, T. Someya, *Science* **2008**, *321*, 1468.

[19] M. Park, J. Im, M. Shin, Y. Min, J. Park, H. Cho, S. Park, M.-B. Shim, S. Jeon, D.-Y. Chung, J. Bae, J. Park, U. Jeong, K. Kim, *Nat. Nano* **2012**, *7*, 803.

[20] M. Park, J. Park, U. Jeong, *Nano Today* **2014**, *9*, 244.

[21] N. Matsuhisa, M. Kaltenbrunner, T. Yokota, H. Jinno, K. Kuribara, T. Sekitani, T. Someya, *Nat. Commun.* **2015**, *6*, 7461.

[22] S. P. Lacour, J. Jones, S. Wagner, T. Li, Z. Suo, *Proc. IEEE* **2005**, *93*, 1459.

[23] S. P. Lacour, D. Chan, S. Wagner, T. Li, Z. G. Suo, *Appl. Phys. Lett.* **2006**, *88*, 204103.

[24] K. Tybrandt, J. Voeroes, *Small* **2016**, *12*, 180.

[25] K. Tybrandt, F. Stauffer, J. Voros, *Sci. Rep.* **2016**, *6*, 25641.

[26] D. Khodagholy, J. N. Gelinas, G. Buzsáki, *Science* **2017**, *358*, 369.

[27] D. Khodagholy, J. N. Gelinas, Z. F. Zhao, M. Yeh, M. Long, J. D. Greenlee, W. Doyle, O. Devinsky, G. Buzsáki, *Sci. Adv.* **2016**, *2*, e1601027.

[28] H. Linden, T. Tetzlaff, T. C. Potjans, K. H. Pettersen, S. Grun, M. Diesmann, G. T. Einevoll, *Neuroendocrinology* **2011**, *72*, 859.

[29] G. Marzun, C. Streich, S. Jendrzej, S. Barcikowski, P. Wagener, *Langmuir* **2014**, *30*, 11928.

[30] C. Pfeiffer, C. Rehbock, D. Hühn, C. Carrillo-Carrion, D. J. de Aberasturi, V. Merk, S. Barcikowski, W. J. Parak, *J. R. Soc., Interface* **2014**, *11*, 20130931.

[31] K. R. Brown, M. J. Natan, *Langmuir* **1998**, *14*, 726.

[32] K.-Y. Chun, Y. Oh, J. Rho, J.-H. Ahn, Y.-J. Kim, H. R. Choi, S. Baik, *Nat. Nano* **2010**, *5*, 853.

[33] P. P. Fu, Q. S. Xia, H. M. Hwang, P. C. Ray, H. T. Yu, *J. Food Drug Anal.* **2014**, *22*, 64.

[34] Y. G. Wang, W. G. Aker, H. M. Hwang, C. G. Yedjou, H. T. Yu, P. B. Tchounwou, *Sci. Total Environ.* **2011**, *409*, 4753.

[35] X. N. Zhu, E. Hondroulis, W. J. Liu, C. Z. Li, *Small* **2013**, *9*, 1821.

[36] L. Guo, M. M. Ma, N. Zhang, R. Langer, D. G. Anderson, *Adv. Mater.* **2014**, *26*, 1427.

[37] D. P. Qi, Z. Y. Liu, Y. Liu, Y. Jiang, W. R. Leow, M. Pal, S. W. Pan, H. Yang, Y. Wang, X. Q. Zhang, J. C. Yu, B. Li, Z. Yu, W. Wang, X. D. Chen, *Adv. Mater.* **2017**, *29*, 1702800.

[38] S. Lacour, S. Benmerah, E. Tarte, J. FitzGerald, J. Serra, S. McMahon, J. Fawcett, O. Graudejus, Z. Yu, B. Morrison III, *Med. Biol. Eng. Comput.* **2010**, *48*, 945.

[39] O. Graudejus, B. Morrison, C. Goletiani, Z. Yu, S. Wagner, *Adv. Funct. Mater.* **2012**, *22*, 640.